Analyst

ROYAL SOCIETY OF CHEMISTRY

PAPER

View Article Online
View Journal

Cite this: DOI: 10.1039/d5an00675a

Carbazole–dansyl conjugate for latent fingerprint visualization and *on-site* detection of date rape drugs

Meghana Sharma,[a] Shagun,[a] Anish Chhillar,[b] Amit Jaiswal *[b] and Abhimanew Dhir *[a]

Received 24th June 2025,
Accepted 24th August 2025

DOI: 10.1039/d5an00675a

rsc.li/analyst

An imino-linked dansyl–carbazole molecular system, **DASH**, is designed and synthesized. This system (**DASH**) is rationalized in such a way that it works as a suitable template for the detection of date rape drugs, *i.e.* gamma-butyrolactone (GBL) and gamma-valerolactone (GVL), in addition to latent fingerprint detection. Both rape drug and latent fingerprint detection are important aspects of drug abuse-related crimes in forensic analysis. There are many reports where both applications have been independently well explored. However, there is no fluorescent system so far that has been reported for dual application. The present study reports the dual application of the molecular system **DASH**, which simultaneously demonstrates *on-site* detection of date rape drugs in the solid state as well as latent fingerprint detection on different surfaces. The biocompatibility of **DASH** is proved utilizing cell viability assay and DNA damage analysis.

1. Introduction

What would be the two most important forensic detection/analysis in a drug-facilitated sexual assault (DFSA)? Of course, the first would be the identification of the illicit drugs[1] or particularly the 'date rape drugs'[2] {gamma-butyrolactone (GBL) and gamma-valerolactone (GVL)} utilized in the assault. Most of these drugs are spiked in beverages so that they can be consumed by the target victim.[2] The second most significant forensic analysis would be the detection, collection, and preservation of latent fingerprints[3,4] as these are one of the most important pieces of evidence in a crime investigation and are significant to legally prove the guilt of the culprit.

Researchers working in the area of fluorescent materials[5,6] have developed all types of novel materials for both applications independently. Particularly for rape drug detection, chromophores based on BODIPY,[7] oxazole,[8] phenol containing α-cynaostilbenes,[9] hydroxyphenyl benzothiazole,[8] and luminescent transition metal complexes;[10] sensing kits; and portable detection kits[11] have been reported. Most of these systems require collection from the crime scene, leading to multiple tests, which may delay the results of the analysis, and the samples require preservation for a longer duration. Therefore, a system that is easily portable and can deliver *on-site* detection is highly desirable.

Recently, aggregation-induced emission (AIE) materials[12] have been well reported for latent fingerprint detection. These include organic AIEgens based on tetraphenylethene,[13] styryl,[14,15] pyridoxal,[16] carbazole,[17,18] amino acid,[19] imidazole[20] and diphenyl pyrimidinones.[21,22] The inorganic systems involve Ir(III),[23,24] Pt(II)[25] and Zn(II)[26] complexes. There are also a few nanomaterials and polymeric materials that are reported for latent fingerprint detection.[27,28] However, most of the fluorescent materials used for the development of latent fingerprints have not been tested for bio-safety. We have given attention to this, and hence, our fluorescent system has been tested for cell viability under different concentrations, confirming its high biocompatibility (*vide infra*).

In the present study, we designed and synthesized a carbazole–dansyl conjugate, **DASH**, which is explored for dual application, *i.e.* rape drug and latent fingerprint detection. The system '**DASH**' is functionalized with a relatively acidic 'H' of 'NH', which is prone to hydrogen bonding and can be an important tool in the detection of both the rape drugs (*vide supra*). The good emission intensity of **DASH** in the solid state generated our interest to evaluate its behavior towards *on-site* detection of rape drugs. These rape drugs are generally spiked in beverages while committing an assault. Chang *et al.*[5] reported the screening parameter of GBL spiked in beverages as 10 mg mL^{-1} with their system. Our system, **DASH**, is efficient enough to detect both the drugs at concentrations much lower than 10 mg mL^{-1} (*vide infra*). In addition, the

[a]*School of Chemical Sciences, Indian Institute of Technology, Mandi, Himachal Pradesh 175005, India. E-mail: abhimanew@iitmandi.ac.in*
[b]*School of Biosciences and Bioengineering, Indian Institute of Technology, Mandi, Himachal Pradesh 175005, India. E-mail: j.amit@iitmandi.ac.in*

presence of two strong fluorophores, 'dansyl' and 'carbazole', in conjugation makes it a potent candidate for latent fingerprint detection.[29,30]

Single molecular systems have been utilized for both the above-mentioned applications, not simultaneously but independently.[5,7,8,29,30] Nevertheless, this could be a limiting factor in DFSA analysis because if different materials are used for these two different applications, complimentary results may not be obtained due to differences in their sensitivity. To exclude any such possibility, the use of a single material is preferable. **DASH** is able to work efficiently in both the applications. Thus, to the best of our knowledge, a carbazole–dansyl conjugate for these dual applications is unprecedented.

2. Experimental section

2.1. Materials and methods

All chemicals and solvents were commercially available and were used without further purification unless otherwise indicated. Dulbecco's modified Eagle's medium (DMEM), fetal bovine serum (FBS), sodium pyruvate, penicillin–streptomycin (pen–strep), and 0.25% trypsin-EDTA were obtained from Thermo Fisher Scientific (Gibco, NY, USA). The cell line was obtained from the National Centre for Cell Science (NCCS), Pune, and further passaged in our laboratory for biological experiments. ^{1}H and ^{13}C NMR spectra were recorded using a JEOL ECX500 MHz spectrometer with TMS as the internal standard. Mass spectra were obtained using an HR-MS Bruker Impact HD. The UV-vis absorption spectra and fluorescence spectra of the compound were recorded using a Shimadzu UV-2450 UV/visible spectrometer and an Agilent fluorescence spectrometer (Cary Eclipse), respectively. Scanning electron microscopy was performed on a Zeiss Gemini SEM 500. A Nikon Eclipse Ti inverted microscope was used for the confocal microscopy, and Nikon NIS-Elements viewer software was used to process the photographs.

2.2. Synthesis of 5-(dimethylamino)-*N*′-((9-phenyl-9*H*-carbazol-3-yl) methylene) naphthalene-1-sulfonohydrazide (DASH)

A solution of **1 (9-Phenyl-9*H*-carbazole-3-carboxaldehyde)** (150 mg, 0.552 mmol) in 4 mL of ethanol was mixed with **2 (Dansyl Hydrazine)** (146.6 mg, 0.552 mmol), and the reaction mixture was refluxed for 2 h until precipitates were formed. The solvent was efficiently removed under vacuum, and the crude product was purified *via* recrystallization using a DCM : EtOH (1 : 1) mixture, resulting in a white solid, designated as **DASH** (Scheme 1); yield 91%; melting point: 210 °C; ^{1}H NMR (500 MHz, $CDCl_3$) δ (ppm): 8.56 (d, J = 8.6, 0.9 Hz, 2H), 8.45 (dd, J = 7.4, 1.3 Hz, 1H), 8.21 (d, J = 1.6 Hz, 1H), 8.08 (dt, J = 7.8, 1.0 Hz, 1H), 7.90 (d, J = 10.2 Hz, 2H), 7.65–7.52 (m, 5H), 7.50–7.45 (m, 3H), 7.40 (m, J = 8.3, 7.0, 1.2 Hz, 1H), 7.35 (dt, J = 8.2, 1.0 Hz, 1H), 7.32–7.27 (m, 1H), 7.17 (dd, J = 7.7, 0.9 Hz, 1H), 2.85 (s, 6H); ^{13}C NMR (125 MHz, $CDCl_3$) δ (ppm): 149.43, 142.46, 141.78, 137.45, 134.26, 131.53, 131.26, 130.37, 128.76, 128.26, 127.44, 126.88, 125.51, 123.76, 123.43, 120.93, 120.88, 120.59, 115.71, 110.47, 110.27, 45.83, 30.10; HRMS: m/z $[M - H]^+$ = 517.175; FTIR (cm^{-1}): 3191 (ν_{-NH}), 2814 ($\nu_{-CH(AR)}$), 2773 ($\nu_{-CH(AL)}$), 1594 ($\nu_{-C=N}$), 1500 ($\nu_{-S=O}$), 1444 (ν_{-CH2}) (Fig. S1–S4).

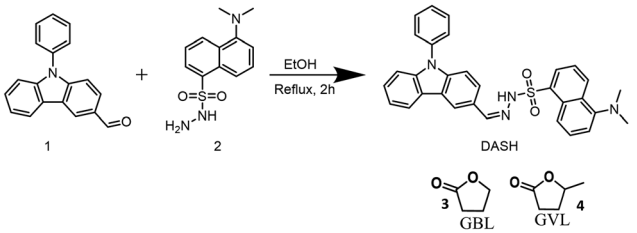

Scheme 1 Synthetic route for **DASH** and chemical structures of GBL and GVL (3 & 4).

2.3. Preparation of DASH@SiO_2 powder and optimization of the procedure for latent fingerprint development

A solution of **DASH** in 5 mL of THF was mixed with nanosilica (pore size: 15 nm), and the reaction mixture was stirred for 30 min. The residual solvent was vacuum-dried, and the resultant mixture was ground to a fine powder using a mortar and pestle. Furthermore, in order to obtain high-contrast LFP images, we optimized the adsorption of **DASH** on silica on the basis of weight percentage. We varied the weight percentage of **DASH** in silica from 0.5% to 10% and named it **DASH@SiO_2**. The powder obtained for each weight percentage of the **DASH** : silica mixture was utilized for developing latent fingerprints on a glass surface.

2.4. Collection and visualization of latent fingerprints

The volunteers washed their hands with soap and ensured the hands were completely dry. Subsequently, fingers were pressed on oily areas of the face (near the nose and forehead). After a 5 min interval, the fingertip was pressed onto various surfaces, including both porous and non-porous materials. **DASH@SiO_2**-based fluorescent powder was dusted over the fingerprint impression. Any excess powder was swiftly removed with a fine brush. The latent fingerprint was subsequently examined under a 365 nm UV lamp, and images were captured using a smartphone.

2.5. Cell viability assay

NIH-3T3 cells were cultured in DMEM supplemented with 10% v/v FBS at 37 °C in a 5% CO_2 incubator. The cytotoxicity of **DASH** was tested using NIH-3T3 cells by MTT-based cell viability assay according to the manufacturer's instructions. The cells were seeded at a density of 10 000 cells per well in a 96-well cell culture plate and allowed to adhere overnight. The following day, the media were discarded from each well, and the cells were treated with **DASH** in a wide range of concentrations (0–40 μg mL^{-1}) for 24 hours. Untreated cells were used as controls. Next, cells were incubated with a specific amount of MTT as per the manufacturer's protocol for 2 hours. Before

taking the readings, the media were removed and 100 μL of DMSO was added to dissolve any insoluble formazan crystals. Finally, the absorbance was recorded at 570 nm using a multi-plate reader. All the experiments were performed in triplicate. The % cell viability was calculated using the following equation:

$$\%\ \text{Cell viability} = \text{Absorbance of treated cells}/\text{Absorbance of untreated cells} \times 100$$

2.6. Electrophoresis characterization

The interaction of **DASH** with DNA was analysed using gel electrophoresis. The reaction solution (10 μL) contained double-stranded GAPDH DNA, different concentrations of **DASH**, and nuclease-free water, and the final concentration of DNA was 0.1 μg μL^{-1}. All the samples were incubated at 37 °C for 1 hour in a Biometra Thermocycler. Then, the samples were run on a 3% agarose gel at 100 V for 1 hour and analysed using a gel documentation system.

3. Results and discussion

To establish the potential of **DASH** as a fluorescent probe, its photophysical properties were thoroughly explored. Fluorescence studies of **DASH** (5.0 mM) were performed in different solvents to ensure if any type of solvatochromism exists. The fluorescence intensity of **DASH** at 5.0 mM concentration in different solvents is shown in Fig. S5. The images of the same solutions under a 365 nm UV illumination are shown in Fig. S6. The data in both the figures reveal the existence of solvatochromism.[31] To further explore its photophysical properties, we investigated the persistence of aggregation-induced emission (AIE).[32–34] The fluorescence spectra of **DASH** (5.0 μM) in different H_2O : MeOH fractions ranging from 0% to 90% were recorded, and the maximum fluorescence intensity was observed in H_2O : MeOH (90 : 10) (Fig. S7 & S8). Aggregation was further confirmed by dynamic light scattering (DLS) and scanning electron microscopy (SEM). The DLS study of **DASH** at 5.0 μM concentration in methanol (MeOH) showed small particles with an average size of 66.17 nm (PDI = 0.4). However, in H_2O : MeOH (90 : 10), the average particle size increased significantly to 295 nm, with a PDI of 0.09 (Fig. S9). This change suggested that the molecules may have aggregated in H_2O : MeOH (90 : 10). Furthermore, the SEM analysis of **DASH** confirmed aggregate formation in the H_2O : MeOH (90 : 10) solvent mixture in comparison to the discrete particles observed in 100% MeOH (Fig. S10).

Drug-facilitated sexual assaults, wherein the beverages are spiked with drugs like GBL and GVL, are one of the prime methods of assaults.[5] The colorless and odorless nature of these drugs makes them prone to be utilized in crimes as beverages could be easily spiked with them to victimize someone. To evaluate whether our fluorescent system could sense both the date rape drugs, we took small amounts of **DASH** samples (6.78 mg and 7 mg) in conical flasks, infused them with GBL (1 μL, native drug sample) or GVL (1.28 μL, native drug sample), and observed them under a 365 nm UV illumination. The fluorescence color of **DASH** changed from blue to yellowish green in both the cases (Fig. 1 I). We performed the same experiment for both the drugs spiked in a beverage. The results obtained in both the cases (*absence and presence of beverages*) were similar (Fig. 1 II). The limit of detection determined for both GBL and GVL was 0.002 μM and 6.45 μM, respectively (Fig. S13 & S14).

One of the most important aspects in forensic analysis is the protection of evidence over a period of time. Therefore, we envisaged that our molecular system could be utilized to test drug-spiked beverages at crime scenes. To evaluate this, we performed a TLC strip experiment, wherein we physically adsorbed **DASH** onto silica-coated aluminum plates. The drugs GVL and GBL were infused in minimum volume (6 μL each) on these **DASH-coated** TLC plates. The infusion of drugs could be immediately detected as the areas on the TLC plates where drug droplets were poured showed a prominent change in color, as observed under a UV torch of 365 nm (Fig. 1 III). Therefore, **DASH** is able to detect both the drugs if beverages spiked with them are found at the crime scene, facilitating the fast outcome of the forensic analysis. Solid-state fluorescence spectrum of **DASH** in the absence and presence of both the drugs was observed at λ_{ex} = 376 nm. The emission band of **DASH** in the presence of equimolar quantities of GBL and GVL showed quenched emission in comparison to **DASH** in the absence of any drug (Fig. 1 IV). Furthermore, to investigate the interaction between **DASH** and drug molecules mechanistically, we performed NMR titration experiments. On addition of an equimolar amount of both the drug samples to **DASH** in DMSO-d_6, its –NH proton signal showed a significant broadness, which is attributed to the interaction between the –NH of **DASH** and hydroxyl groups[35] present in both the drug molecules (Fig. S12).

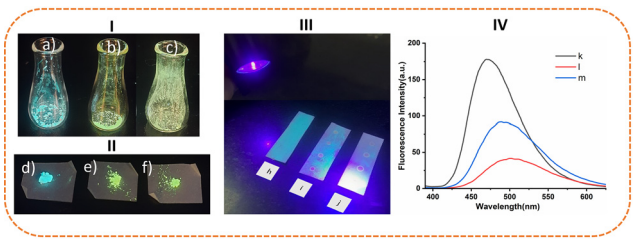

Fig. 1 (I) Visual detection of drugs: (a) **DASH**; (b) **DASH** (6.78 mg) with GBL (1 μL, native drug sample); and (c) **DASH** (7 mg) with GVL (1.28 μL, native drug sample) under a 365 nm UV illumination. (II) Detection of drugs in spiked drinks: (d) **DASH**; (e) **DASH** (6.78 mg) with GBL (1 μL, native drug sample); and (f) **DASH** (7 mg) with GVL (1.28 μL, native drug sample) under a 365 nm UV illumination. (III) Drug detection using the TLC strip method under a UV torch of 365 nm illumination: (h) **DASH** adsorbed on a TLC strip; (i) GBL infused on a **DASH**-coated TLC strip; and (j) GVL infused on a **DASH**-coated TLC strip. (IV) Fluorescence spectra of **DASH** (k) and upon addition of equimolar concentrations of GBL (l) (0.0135 mmol) and GVL (m) (0.0135 mmol).

We further investigated the properties of **DASH** for latent fingerprinting application. To get more uniformity in terms of particle size, we prepared nanosilica-adsorbed **DASH** in different weight percents ranging from 0.5% to 10% (Fig. 2a), referred to as **DASH@SiO$_2$** (*vide supra*). The rationale was to optimize the best latent fingerprinting results with a minimum amount of **DASH**. The latent fingerprints taken on glass substrates were developed with different weight percent fractions of **DASH** adsorbed on silica. The best results with the brightest fluorescence were observed using 10 weight percent of **DASH** (Fig. 2a & b). The solid-state fluorescence (λ_{ex} = 376 nm) for each of the weight percent is represented in Fig. 2c. This 10 percent weight fraction of **DASH@SiO$_2$**, hereafter referred to as **10%DASH@SiO$_2$**, was further utilized to observe latent fingerprints on other surfaces *viz.* a glass bottle, ceramic, aluminum foil, knife, coin and CD (Fig. 3).

10%DASH@SiO$_2$ used to develop latent fingerprints on CD was further utilized to elucidate different level details of fingerprints. The central image in Fig. 4 represents the different levels of latent fingerprints. The level details are encircled in different colors: red color-arch (**L-1**), orange color-bifurcations (**L-2**), yellow color-ridge crossings (**L-2**), pink color-lakes (**L-2**), and white color-pores (**L-3**). The enlarged images of these levels are represented on either side of the central image. Therefore, **DASH** is able to detect and differentiate between different levels of latent fingerprints (LFPs) with high resolution and contrast without any pre- or post-chemical and physical treatments.

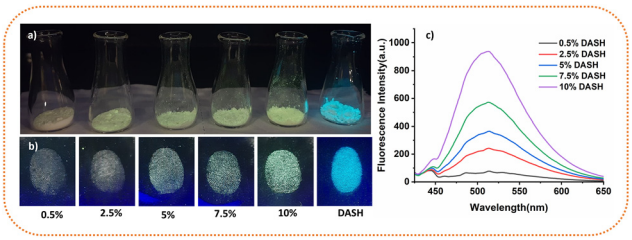

Fig. 2 (a) Conical flasks containing different fractions of **DASH** adsorbed on silica and **DASH** alone under a 365 nm UV illumination. (b) Latent fingerprint images developed using different wt% of **DASH@SiO$_2$** and **DASH** on glass slides. (c) Fluorescence spectra of different fractions of **DASH** adsorbed on silica.

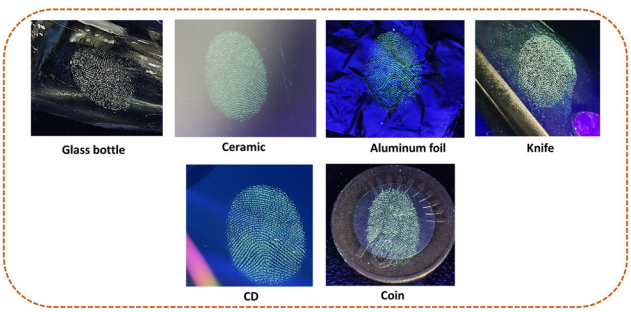

Fig. 3 Latent fingerprints developed with **10%DASH@SiO$_2$** on different substrates under a 365 nm UV illumination.

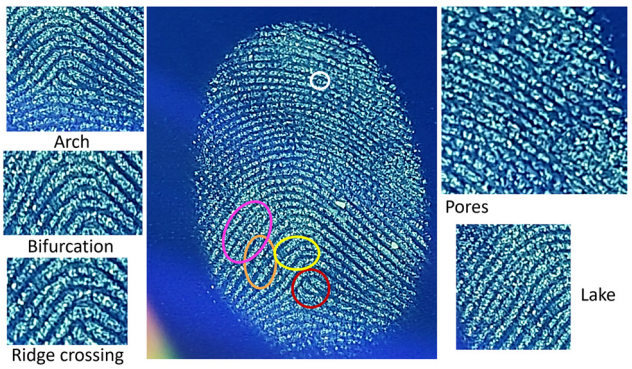

Fig. 4 Central image of the index finger representing different levels observed in latent fingerprint detection using **10%DASH@SiO$_2$**. The different level details are encircled in different colors, red circle represents an Arch (**L-1**), orange bifurcations (**L-2**), yellow ridge crossing (**L-2**), pink lake (**L-2**), white color pores (**L-3**). The enlarged images of these levels are represented at either side of the central image.

SEM images of the fingerprints generated more elevated details of different levels of latent fingerprints, which include ridge intervals and intervals between pores. This is evident from Fig. S16(a & b), where incomplete ridges are visualized, while in the presence of **10%DASH@SiO$_2$** (Fig. S16(c & d)), complete ridges could be easily observed with high clarity, confirming the significant role of **10%DASH@SiO$_2$** in elevating the details of latent fingerprints. Similar results were observed in optical microscopy (Fig. S18). This clarity of the ridges in the presence of **10%DASH@SiO$_2$** was further confirmed by confocal microscopy images, where the blue fluorescent ridges could be seen (Fig. S19b) with brighter and better resolution than ridges in the absence of **10%DASH@SiO$_2$** (Fig. S19a). Latent fingerprints were developed using black magnetic powder, which showed good development on bright surfaces (Fig. S20a & d) and poor development on darker surfaces (Fig. S20b & c). On the contrary, **10%DASH@SiO$_2$** showed a consistent development of latent fingerprints irrespective of the contrasting surfaces (Fig. S20e–h). Similarly, we performed comparative analysis with pyrene,[36] 1,8-naphthalimide[37] and anthracene.[38] The fingerprints developed with **10% DASH@SiO$_2$** were much more prominent because of its bright yellow-green fluorescence (Fig. S21). Latent fingerprints at crime scenes are often susceptible to environmental factors such as moisture and heat, which may affect their visibility and development. To assess the robustness and effectiveness of **10%DASH@SiO$_2$** in detecting fingerprints exposed to such conditions, we conducted a series of controlled experiments. Different fingerprints were initially pressed onto glass substrates and subjected to aquatic conditions for a few minutes to simulate exposure to moisture. After this, the samples were dried under direct sunlight for 15 minutes and further placed in a hot air oven at 80 °C to evaluate the impact of sustained heat exposure. Finally, **10%DASH@SiO$_2$** was spread over the fingerprints to facilitate visualization. Observations confirmed that the effectiveness of **10%DASH@SiO$_2$** remained unchanged as it successfully developed fingerprints despite prior exposure

to both water and heat (Fig. S22a–f), reaffirming its reliability in challenging forensic scenarios. All the above experiments were performed as per the guidelines produced by the International Fingerprint Research Group IFRG[39] (Fig. S15, S17, S22 and S23). We also tested different natural fingermarks across multiple substrates and under different environments (*vide supra*). Details of the natural mark study, including substrate variation and moisture and heat control, are provided in the supplementary section (Fig. S15 & S22).

Preserving fingerprints over time is important in forensic investigations. For our experiment, we developed latent fingerprints (LFPs) on glass surfaces using **10%DASH@SiO$_2$** that were left for 1 day, 7 days, 14 days, 21 days and 28 days. Over the period of 28 days, the latent fingerprints were almost similar to those on day 1. All levels of details (level 1 to level 3) of the fingerprints, *viz.* ridges, pores and arches, were visible (Fig. S24). This highlights the stability of the latent fingerprints in the presence of **10%DASH@SiO$_2$**, proving it as a strong candidate for forensic applications.

The evaluation of the biocompatibility of **DASH** and its impact on DNA integrity was conducted through MTT assay and agarose gel electrophoresis, respectively. NIH-3T3 cells were treated with various concentrations of DASH dye ranging from 0–40 μg mL^{-1} for 24 h. After the removal of the treatment media, the cellular viability of the treated cells was then determined by MTT-based cell viability assay. The results of the MTT assay clearly indicated a high cell viability up to more than 82%. This finding indicates that **DASH** exhibits excellent biocompatibility and minimal cytotoxicity (Fig. 5a), suggesting that **DASH** is relatively safe for potential applications in latent DNA fingerprinting. Furthermore, for any dye to be used for criminal investigations, it must be DNA-friendly and should not damage the genetic material.[40] So, to evaluate the potential of **DASH** to be used in latent fingerprinting, agarose gel electrophoresis was performed. **DASH** in different molar ratios was incubated with double-stranded DNA to examine whether any DNA degradation or DNA hydrolysis into fragments was taking place. As depicted in Fig. 5b, intact bands of DNA at the same position as that of the control were observed in all the treated conditions, confirming that **DASH** did not cause any DNA damage. Collectively, these results underscore the potential of **DASH** as a safe, non-toxic, and effective agent for latent fingerprinting visualization. Its non-toxicity and lack of detrimental effects on DNA make it a potential candidate for forensic applications.

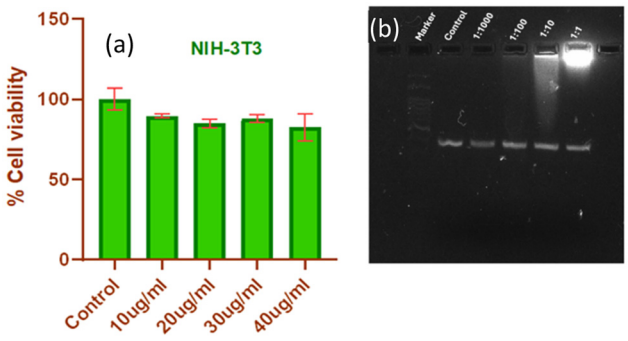

Fig. 5 (a) Cell viability of cells treated with different concentrations of DASH for 24 h in NIH-3T3 cell lines. (b) Agarose gel electrophoresis of DNA. Lane 1: the marker (reference for the size of the DNA fragment); lane 2: DNA only; lane 3–6: DNA treated with **DASH** with molar ratio of DNA : **DASH** = 1 : 1000, 1 : 100, 1 : 10, and 1 : 1, respectively.

4. Conclusions

To conclude, we have designed and synthesized a carbazole–dansyl conjugate that exhibits selective *on-site* detection of date rape drugs and latent fingerprints with good resolution. The material is also biocompatible, ensuring the safety of investigators. This work may prompt researchers to reinvestigate and look for new functional materials for forensic applications.

Author contributions

Meghana Sharma: investigation, methodology, data curation, writing – original draft, Shagun: validation and visualization, Anish Chhillar: methodology, data curation, writing – original draft (biological), Amit Jaiswal: supervision, writing-review and editing (biological), Abhimanew Dhir: conceptualization, supervision, resources, writing-review and editing.

Conflicts of interest

There are no conflicts to declare.

Data availability

The data supporting this article have been included as part of the SI.

The SI includes spectroscopic characterization and ^{1}H NMR titrations, fluorescent spectra and images under different conditions, SEM, Optical and Confocal Microscopy, LOD, comparison with commercial and other dye residues for latent fingerprinting. See DOI: **https://doi.org/10.1039/d5an00675a**.

Acknowledgements

MS extends heartfelt thanks to the Indian Institute of Technology, Mandi, for the research fellowship and the Advanced Materials Research Centre (AMRC), IIT Mandi, for the research facilities. AD acknowledges IIT Mandi for project IITM/SG/2023-06-1659.

References

1 R. Pal and A. Teotia, *Int. J. Med. Toxicol. Leg. Med.*, 2010, **12**, 36.
2 C. M. Beynon, C. McVeigh, J. McVeigh, C. Leavey and M. A. Bellis, *Trauma Violence Abuse*, 2008, **9**, 178.
3 G. L. Thomas, *J. Phys. E:Sci. Instrum.*, 1978, **11**, 722.

4 B. Scruton, B. W. Robins and B. H. Blott, *J. Phys. D: Appl. Phys.*, 1975, **8**, 714.
5 D. Zhai, B. K. Agrawalla, P. Sze, F. Eng, S.-C. Lee, W. Xu and Y.-T. Chang, *Chem. Commun.*, 2013, **49**, 6170.
6 M. Wang, M. Li, A. Yu, Y. Zhu, M. Yang and C. Mao, *Adv. Funct. Mater.*, 2017, **27**, 1606243.
7 S. Rodríguez-Nuévalos, A. M. Costero, M. Parra, S. Gil, P. Arroyo, J. A. Sáez, P. Gaviña, P. Ceroni and A. Fermi, *Dyes Pigm.*, 2022, **207**, 110757.
8 N. Anzar, S. Suleman, S. Parvez and J. Narang, *Process Biochem.*, 2022, **113**, 113.
9 R. Dahiwadkar, H. Kumar and S. Kanvah, *J. Photochem. Photobiol., A*, 2022, **427**, 113844.
10 G. Li, C. Wu, D. L. Ma and C. H. Leung, *TrAC, Trends Anal. Chem.*, 2021, **139**, 116270.
11 S. U. Son, S. Jang, B. Kang, J. Kim, J. Lim, S. Seo, T. Kang, J. Jung, K. S. Lee, H. Kim and E. K. Lim, *Sens. Actuators, B*, 2021, **347**, 130598.
12 Y. Li, L. Xu and B. Su, *Chem. Commun.*, 2012, **48**, 4109.
13 X. Jin, R. Xin, S. Wang, W. Yin, T. Xu, Y. Jiang, X. Ji, L. Chen and J. Liu, *Sens. Actuators, B*, 2017, **244**, 777.
14 S. Chadwick, P. Maynard, P. Kirkbride, C. Lennard, A. McDonagh, X. Spindler and C. Roux, *Forensic Sci. Int.*, 2012, **219**, 208.
15 X. Jin, L. Dong, X. Di, H. Huang, J. Liu, X. Sun, X. Zhang and H. Zhu, *RSC Adv.*, 2015, **5**, 87306.
16 V. Bhardwaj, S. K. A. Kumar and S. K. Sahoo, *Microchem. J.*, 2022, **178**, 107404.
17 Y. Chen, A. Li, X. Li, L. Tu, Y. Xie, S. Xu and Z. Li, *Adv. Mater.*, 2023, **35**, 2211917.
18 S. Li, L. Wang, Y. Ma, L. Zhu and W. Lin, *Sens. Actuators, B*, 2022, **371**, 132595.
19 P. Singh and P. Sharma, *Tetrahedron Lett.*, 2020, **61**, 151698.
20 M. K. Ravindra, K. M. Mahadevan, R. B. Basavaraj, G. P. Darshan, S. C. Sharma, M. S. Raju, G. R. Vijayakumar, K. B. Manjappa, D. Y. Yang and H. Nagabhushana, *Mater. Sci. Eng., C*, 2019, **101**, 564.
21 H. Singh, R. Sharma, G. Bhargava, S. Kumar and P. Singh, *New J. Chem.*, 2018, **42**, 12900.
22 P. Singh, H. Singh, R. Sharma, G. Bhargava and S. Kumar, *J. Mater. Chem. C*, 2016, **4**, 11180.
23 Z. Song, R. Liu, X. Li, H. Zhu, Y. Lu and H. Zhu, *J. Mater. Chem. C*, 2018, **6**, 10910.
24 L. Di, Y. Xing, Z. Yang and Z. Xia, *Sens. Actuators, B*, 2022, **350**, 130894.
25 C. Li, L. Xu, J. Li, X. Chen, Z. Chi, B. Xu and J. Zhao, *Dyes Pigm.*, 2023, **209**, 110912.
26 L. Duan, Q. Zheng and T. Tu, *Adv. Mater.*, 2022, **34**, 2202540.
27 X. Xu, L. Mo, Y. Li, X. Pan, G. Hu, B. Lei, X. Zhang, M. Zheng, J. Zhuang, Y. Liu, C. Hu, X. Xu, L. Mo, Y. Li, X. Pan, B. Lei, X. Zhang, M. Zheng, J. Zhuang, Y. Liu, C. Hu and G. Hu, *Adv. Mater.*, 2021, **33**, 2104872.
28 R. Zou, Y. Yu, H. Pan, P. Zhang, F. Cheng, C. Zhang, S. Chen, J. Chen and R. Zeng, *ACS Appl. Mater. Interfaces*, 2022, **14**, 16746.
29 P. Li, Z. Q. Zhou, L. H. Liu, B. Y. Ji, H. R. Song, J. Y. Luan, G. Q. Xiang, Y. Fang, S. Chen, K. P. Wang and Z. Q. Hu, *Dyes Pigm.*, 2024, **228**, 112214.
30 L. F. A. M. Oliveira, L. V. A. T. da Silva, A. F. Sonsin, M. S. Alves, C. V. Costa, J. C. S. Melo, N. Ross, P. T. Wady, T. Zinn, T. G. do Nascimento, E. J. S. Fonseca, A. M. L. de Assis, A. R. Hillman and A. S. Ribeiro, *RSC Adv.*, 2024, **14**, 22504.
31 A. Marini, A. Muñoz-Losa, A. Biancardi and B. Mennucci, *J. Phys. Chem. B*, 2010, **114**, 17128.
32 Y. Hong, J. W. Y. Lam and B. Z. Tang, *Chem. Commun.*, 2009, 4332.
33 Y. Chen, W. J. Y. Lam, T. R. K. Kwok, B. Liu and B. Z. Tang, *Mater. Horiz.*, 2019, **6**, 428.
34 Z. Zhao, H. Zhang, W. Y. Lam and B. Z. Tang, *Angew. Chem., Int. Ed.*, 2020, **59**, 9888.
35 M. Brutschy, M. W. Schneider, M. Mastalerz and S. R. Waldvogel, *Chem. Commun.*, 2013, **49**, 8398.
36 A. Shabashini, S. Richard, M. K. Panda, S. K. Panja and G. C. Nandi, *Mater. Adv.*, 2024, **5**, 1099.
37 S. Kumar and P. Singh, *J. Photochem. Photobiol., A*, 2023, **437**, 114418.
38 C. Worawong, W. Phutdhawong, S. Jirasirisuk and W. Phutdhawong, *Chem. Sci. Trans.*, 2015, **4**, 1043.
39 J. Almog, A. A. Cantu, C. Champod, T. Kent and C. Lennard, Guidelines for the Assessment of Fingermark Detection Techniques, *J. Forensic Identif.*, 2014, **64**, 174.
40 Y. Fang, J. Y. Luan, J. S. Zhao, X. R. Kao, H. R. Song, Y. N. Luo, K. P. Wang, S. Chen, H. Y. Hu and Z. Q. Hu, *Chin. J. Chem.*, 2024, **42**, 3337.